Hindawi
International Journal of Antennas and Propagation
Volume 2018, Article ID 2472738, 13 pages
https://doi.org/10.1155/2018/2472738

Research Article

Analysis and Synthesis of Double Negative Dielectric Media Rectenna Systems for Ambient Microwave Energy Harvesting

Apostolia Karampatea and Katherine Siakavara

Radiocommunications Laboratory, School of Physics, Aristotle University of Thessaloniki, 54124 Thessaloniki, Greece

Correspondence should be addressed to Katherine Siakavara; skv@auth.gr

Received 19 September 2017; Revised 9 December 2017; Accepted 1 January 2018; Published 28 March 2018

Academic Editor: Ding-Bing Lin

The concept of harvesting the ambient electromagnetic radiation energy, coming from public telecommunication wireless networks, has been recently subject of extensive research. Techniques proposed for this target use mainly antennas, as the grade gathering the radiation power. In this work, a method introducing the usage of specific dielectric structures with artificially negative electric permittivity and magnetic permeability (double negative media or DNG) in combination with wire dipole antenna sensors is proposed as an RF harvesting system. Theoretical study of the synthesized DNG medium's performance and the distribution of the electromagnetic field in its interior is made, with the intention of finding the areas of maximum electric field intensity at which the antenna sensors would be positioned for maximum power scavenging. The received numerical results show that the synthesized schemes are capable of enhancing the energy gathering ability. Compared to the same antenna sensors positioned in free space, they ensure higher input voltage to the rectifier and also an increase of the available power about 10 dB. Moreover, they exhibit this performance for every direction of arrival of the incoming waves. The hybrid schemes DNG dipole antenna were designed for the Universal Mobile Telecommunication System (UMTS) frequency band, but the method is general and would be applied to any other frequency band and also with other antenna types.

1. Introduction

The ambient energy harvesting has been evolved as enable technology for smart environments (Internet of things, smart cities, etc.) at which devices with self-sustainable electric power operation are important. For this purpose, research has been focused to harvesting energy from ambient resources as vibration, solar, wind, heat, and radio-frequency (RF) signals. Among them, the scavenging of RF energy has several advantages, compared to rest of resources, and a drawback as well. RF energy is twenty-four hours present in the environment coming from public telecommunication networks, as cellular GSM (890–910 MHz), DCS/PCS/UMTS (1800–2100 MHz), WiFi (2.45 GHz), WLANs, Digital TV in UHF, and also at lower frequency bands as FM radio [1–4]. All these resources are not only continuously available, but are also free, exist either way, due to wireless services offered to the public, and their harvesting constitutes substantially a recycling of the respective RF energy. The single drawback of the RF energy could be that, among the above mentioned resources, it is the one with the lowest power level in the ambient, exhibiting power density about 0.2 nW/cm^2–1 μW/cm^2.

The main units of an RF power collective scheme are (a) the element that captures efficiently the ambient energy, being, in practice, an antenna, (b) a rectifying circuit that converts the gathered AC electromagnetic energy to direct current (DC) energy, and (c) a device that stores the DC energy. A great variety of schemes which include the first two grades of a harvesting system have been proposed in the literature, and the majority of them introduce antennas of printed type incorporated with rectifying units [5–12]. Moreover, effective solutions with metamaterial or fractal concept-inspired antennas [13–15], with dielectric resonators [16, 17] and metasurface closed ring arrays [18], have also been presented.

In the present work, taking into account the low levels of the ambient RF power, a technique is proposed for the synthesis of rectenna systems at which the sensors, for collecting the power, are embedded in a material which when excited by the ambient RF waves, has the capability to develop in its interior electromagnetic fields of high intensity. In this way, the sensors, exposed to high-strength field environment, obtain to increase the amount of gathered power. As material of this type, a DNG structure was synthesized, and as sensors, simple linear wire dipoles incorporated in its interior were used. The artificial DNG materials are usually periodic structures composed of, for example, microstrip elements of specific layout and arrangements of open printed metallic rings or pins with suitable size and disposition or they are of hybrid dielectric type composed of a homogeneous dielectric host inside which periodic lattices of dielectric particles with different dielectric constant are embedded. Whatever type the metamaterial structure is, it has a basic attribute common to all the rest types. When an electromagnetic wave propagates through it, it experiences negative phase velocity and positive group velocity. This performance would lead to features of operation exploitable in many applications. In the present work, the hybrid dielectric type DNG was selected because it has, additionally, the capability of increasing the intensity level of ambient signals incident on the harvesting scheme, due to the resonance of the dielectric particles. The synthesis and the study of the entire scheme were made for the UMTS band.

The rest of the paper is organized as follows. In Section 2, a short presentation of the DNG structure's performance concerning its effective permeability and permittivity is presented, and then the theoretical evaluation of the electromagnetic field inside a DNG structure is analyzed. The evaluation was made via the phenomenon and the respective theory of the resonance of a dielectric particle when it is illuminated by a plane wave. The produced mathematical formulae were used for the numerical evaluation of the field inside the DNG and the verification of high-field intensity levels in the interior and the vicinity of the DNG. Section 3 includes all the numerical results concerning (a) the performance of the DNG and the verification of the resonance of its particles, (b) the electric field intensity distribution in the interior of the DNG, calculated theoretically and via simulation, which shows the positions of maximum field intensity, and (c) the performance of the linear wire dipole sensors embedded in the DNG and in detail all the numerical results regarding the proportion of the gathered energy that is available to the rectifier. A simple full wave rectifier was used which, as it is well known, during the conversion from ac to dc has effectiveness ~81%. This percentage value would increase using a multiple-stage rectifier or a rectifier of special synthesis. However, the entire present work has focused on the synthesis of a novel hybrid sensor of DNG-dipoles, the investigation of its attributes, and its ability of gathering satisfactory high amount of ambient EM power and also effectively transferring this power to a rectifier as an ac signal, namely, before the conversion to dc and moreover to ensure sufficient voltage level to the rectifier's input. So, the synthesis of a novel rectifier was out of scope at this step. Finally, the conclusions are included in Section 4.

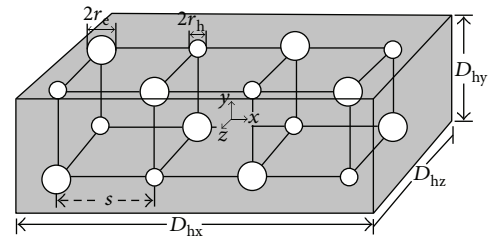

Figure 1: The global lattice composed of two bisphere overlapping lattices of the dielectric particles with different radius sizes embedded inside the dielectric host (Lattice A).

2. Theoretical Analysis

2.1. The Artificial DNG Structure and Performance. Generally, a medium consisting of a lattice of insulating dielectric spherical particles with specific dielectric constant, embedded in an homogeneous dielectric host of dielectric constant much smaller than that of the particles, constitutes a hybrid inhomogeneous medium with special attributes. When a wave propagates through it, experiences the host and the lattice as an equivalent homogeneous medium having an effective permittivity ε_{eff} or/and permeability μ_{eff}, with negative sign, on condition that the size and the dielectric constants of the particles as well as the dielectric constant of the host are properly selected. This selection is based on the theoretical model of the artificial metamaterials [19–21]. For the propagation of a wave through them to be feasible, both the above parameters have to be negative and the medium is termed as DNG. A classical DNG model which produces structures that would permit the propagation of the signals and at the same time its fabrication would be feasible is an isotropic artificial DNG material, composed of two sets of dielectric spherical particles, which form two periodic lattices embedded in a dielectric material host. The particles are made from the same or different double positive (DPS) dielectric material with dielectric constant much larger than that of the host and have different radii. The wavelength inside the particles is comparable with their diameter and at the same time the wavelength outside of them is large compared to their inter-distances. Each set of equally spaced spherical particles constitutes a 3D lattice and the two lattices overlap in a way that the particles do not overlap (Figure 1). An electromagnetic wave impinging on this complex structure excites simultaneously TE modes in the smaller sphere and TM modes in the larger ones, at the frequencies which are close to the spherical cavity eigenfunctions. Respective theoretical full wave analysis which concerns the proposed DNG is presented in Section 2.2. The averaging of the magnetic momentum corresponding to TM_{011} mode and the electric momentum of the TE_{011} mode, over the cells of the spherical particles, reveals the negative permeability and the permittivity correspondingly [19–21].

The aforementioned concepts and conditions were adopted by Lewin [19, 20] in the modeling of electromagnetic response of spherical inclusions, with intention to produce the effective relative permittivity and permeability of an artificial DNG scheme, and are presented in the approximate expressions (1).

$$\varepsilon_{\text{eff}} = \varepsilon_h \left(1 + \frac{3v_{fe}}{(F_e(\theta) + 2b_e)/(F_e(\theta) - b_e) - v_{fe}}\right),$$
$$\mu_{\text{eff}} = \mu_h \left(1 + \frac{3v_{fm}}{(F_m(\theta) + 2b_m)/(F_m(\theta) - b_m) - v_{fm}}\right). \tag{1}$$

In the above expressions, the parameters are defined as $b_e = \varepsilon_h/\varepsilon_p$ and $b_m = \mu_h/\mu_p$, where ε_h and ε_p are the relative permittivity and μ_h and μ_p are the relative permeability of the host medium and the particles; the volume fractions v_{fe} and v_{fm} are defined as $v_{fe,fm} = 4\pi r_{pe,pm}^3/(3p_{e,m}^3)$, where $r_{pe,pm}$ are the radii of the particles, $p_{e,m}$ is the particle spacing, and $F_{e,m}(\theta) = 2(\sin(\theta_{e,m}) - \theta\cos(\theta_{e,m}))/((\theta_{e,m}^2 - 1)\sin(\theta_{e,m}) + \theta\cos(\theta_{e,m}))$, where $\theta_{e,m} = k_0 r_{pe,pm}\sqrt{\varepsilon_{pe}\mu_{pm}}$, and $k_0 = 2\pi/\lambda$ is the free space wave number. The exact values of the particles' radii, for resonance, can be also theoretically ascertained, as in the next subsection is presented.

2.2. Theoretical Evaluation of the Electromagnetic Field inside the DNG Structure. As in Section 2.1 was mentioned, the target of the present work was the exploitation of the high electromagnetic field values arising inside the DNG structure in order that we would gather, via sensors, the electromagnetic power of a plane wave impinging on it. For the selection of the suitable position of the sensors, it is essential to find out the areas, inside which the field is maximized. It is understood that the field is maximized in the interior of resonant particles. However, it is not the right place for the sensors, because if they penetrate the particles, the excitation of the resonances is prevented. So, the regions of the structure with satisfactory high field values are searched for, inside the host and outside the particles. In practice, DNG structure and sensors are illuminated by plane waves of frequencies inside the selected band. Consequently, the first step of the study is to find the field excited inside the DNG, firstly without sensors, when a plane wave impinges on it. In accordance with the theory in [22], a primary periodic wave incident upon a dielectric sphere sets up a secondary field both inside and outside the sphere, and the resultant field at any point is the vector sum of the primary and secondary fields. Referring to Figure 1 and for anyone of the dielectric particles, embedded in the host, we define its radius r_p and define as propagation constant k_1, that is inside to the sphere and as k_2 the respective constant inside the host. Moreover, we suppose that the host medium is extended to infinity. Under these conditions, we suppose that a plane wave, whose electric vector is linearly polarized in the x-direction, propagates inside the host in the direction of positive z-axis and falls upon to the selected sphere. The expansion of this incident field in vector spherical wave functions [22] is

$$\mathbf{E}^i = \mathbf{x}E_0 e^{i(\omega t - k_2 z)} \xrightarrow[\text{wave functions}]{\text{spherical}} \mathbf{E}^i(r,\theta,\varphi)$$
$$= E_0 e^{i\omega t}\sum_{n=1}^{\infty} i^n \frac{2n+1}{n(n+1)}\left(\mathbf{m}_{o1n}^{(1)} - i\mathbf{n}_{e1n}^{(1)}\right),$$
$$\mathbf{H}^i = \hat{y}\frac{k_2}{\mu_2\omega}E_0 e^{i(\omega t - k_2 z)}$$
$$= -\frac{k_2 E_0 e^{i\omega t}}{\mu_2\omega}\sum_{n=1}^{\infty} i^n \frac{2n+1}{n(n+1)}\left(\mathbf{m}_{e1n}^{(1)} + i\mathbf{n}_{o1n}^{(1)}\right), \tag{2}$$

where E_0 is the amplitude, $\mathbf{r}(r,\theta,\varphi)$ is the position at which the field is considered, and

$$\mathbf{m}_{\substack{o\\e}1n}^{(1)}(\bar{r}) = \pm\frac{1}{\sin\theta}J_n(k_2 r)P_n^1(\cos\theta)_{\sin}^{\cos}\varphi\,\hat{\theta} - J_n(k_2 r)\frac{\partial P_n^1}{\partial\theta}{}_{\cos}^{\sin}\varphi\,\hat{\varphi},$$
$$\mathbf{n}_{\substack{o\\e}1n}^{(1)}(\mathbf{r}) = \frac{n(n+1)}{k_2 r}J_n(k_2 r)P_n^1(\cos\theta)_{\sin}^{\cos}\varphi\,\hat{r}$$
$$+\frac{1}{k_2 r}\left[k_2 r J_n(k_2 r)\right]'\frac{\partial P_n^1}{\partial\theta}{}_{\cos}^{\sin}\varphi\,\hat{\theta}$$
$$\pm\frac{1}{k_2 r\sin\theta}\left[k_2 r J_n(k_2 r)\right]' P_n^1(\cos\theta)_{\sin}^{\cos}\varphi\,\hat{\varphi}. \tag{3}$$

In the above equations, the prime denotes differentiation with respect to argument; $k_2 r$ and J_n are spherical Bessel functions of the first kind, and P_n^1 is related to the first derivative of associated Legendre polynomial of nth degree.

The induced secondary field must be constructed in two parts, the one excited to the interior of the sphere and the other valid at all external points. These two parts are described by (4), (5), (6), and (7).

For $r > r_p$ holds that

$$\mathbf{E}^r(r,\theta,\varphi,r_p) = E_0 e^{i\omega t}\sum_{n=1}^{\infty} i^n \frac{2n+1}{n(n+1)}\left(a_{rn}\mathbf{m}_{o1n}^{(3)} - ib_{rn}\mathbf{n}_{e1n}^{(3)}\right), \tag{4}$$

$$\mathbf{H}^r(r,\theta,\varphi,r_p) = -\frac{k_2 E_0 e^{i\omega t}}{\mu_2\omega}\sum_{n=1}^{\infty} i^n \frac{2n+1}{n(n+1)}\left(b_{rn}\mathbf{m}_{e1n}^{(3)} + ia_{rn}\mathbf{n}_{o1n}^{(3)}\right), \tag{5}$$

where functions $\mathbf{m}_{\substack{o\\e}1n}^{(3)}$ and $\mathbf{n}_{\substack{o\\e}1n}^{(3)}$ are obtained by replacing $J_n(k_2 r)$ by $h_n^{(1)}(k_2 r)$, which is the spherical Hankel function of the first kind and k_2 by k_1, in the formulae of $\mathbf{m}_{\substack{o\\e}1n}^{(1)}$ and $\mathbf{n}_{\substack{o\\e}1n}^{(1)}$ shown above. For $r < r_p$ holds that

$$\mathbf{E}^t(r,\theta,\varphi,r_p) = E_0 e^{i\omega t}\sum_{n=1}^{\infty} i^n \frac{2n+1}{n(n+1)}\left(a_{tn}\mathbf{m}_{o1n}^{(1)} - ib_{tn}\mathbf{n}_{e1n}^{(1)}\right), \tag{6}$$

$$\mathbf{H}^t(r,\theta,\varphi,r_p) = -\frac{k_1 E_0 e^{i\omega t}}{\mu_1 \omega}\sum_{n=1}^{\infty} i^n \frac{2n+1}{n(n+1)}\left(b_{tn}\mathbf{m}_{e1n}^{(1)} + ia_{tn}\mathbf{n}_{o1n}^{(1)}\right). \tag{7}$$

The unknown coefficients a_{rn}, b_{rn}, a_{tn}, and b_{tn} are determined by the equations coming from the boundary conditions for the electric and magnetic fields applied on the sphere's surface, namely, for $r = r_p$. The solutions of the equations give

$$\begin{aligned}
a_{rn}(r_p) &= \frac{\mu_1 J_n(k_1 r_p)\left[k_2 r_{po} J_n(k_2 r_p)\right]' - \mu_2 J_n(k_2 r_p)\left[k_1 r_p J_n(k_1 r_p)\right]'}{\mu_1 J_n(k_1 r_p)\left[k_2 r_p h_n^1(k_2 r_p)\right]' - \mu_2 h_n^1(k_2 r_p)\left[k_1 r_p J_n(k_1 r_p)\right]'},\\
b_{rn} &= -\frac{\mu_1 J_n(k_2 r_p)\left[k_1 r_0 J_n(k_1 r_p)\right]' - \mu_2 (k_1/k_2)^2 J_n(k_1 r_p)\left[k_2 r_p J_n(k_2 r_p)\right]'}{\mu_1 h_n^1(k_2 r_p)\left[k_1 r_p h_n^1(k_1 r_p)\right]' - \mu_2 (k_1/k_2)^2 J_n(k_1 r_p)\left[k_2 r_p h_n^1(k_1 r_p)\right]'},\\
a_{tn} &= \frac{\left(J_n(k_2 r_0) + a_{rn} h_n^1(k_2 r_0)\right)}{\left(J_n(k_1 r_0)\right)},\\
b_{tn} &= \frac{\mu_1\left(J_n(k_2 r_0) + b_{rn} h_n^1(k_2 r_0)\right)}{\left[\mu_2 (k_1/k_2) J_n(k_1 r_0)\right]}.
\end{aligned} \tag{8}$$

All the above are valid for one dielectric particle. If we consider the lattice shown in Figure 1 composed of three DNG cells, the intensity of total electric field at a point (x_0, y_0, z_0) inside the host but outside from any particle is the summation of the incident field intensity and the field intensities produced by the total number, N_p, of the particles. For an approximate assessment and without taking into account the interaction among the particles, this intensity is described by the following equation:

$$\mathbf{E}(R_0) = \mathbf{E}^i(\mathbf{R}_0) + \sum_{j=1}^{N_p} \mathbf{E}^r\left(\mathbf{R}_{0j}, \mathbf{r}_p^j\right), \tag{9}$$

where $\mathbf{R}_0(x_0, y_0, z_0)$ is the position vector of the point of interest with respect to the coordinate system localized at the center of the entire lattice, $\mathbf{R}_{0j}(x_0, y_0, z_0 \mid x_j, y_j, z_j)$ is the position vector of the point of interest with respect to the position of the jth dielectric particle defined as $\mathbf{R}_{0j}(x_0, y_0, z_0 \mid x_j, y_j, z_j) = \mathbf{R}_0(x_0, y_0, z_0) - \mathbf{r}_j(x_j, y_j, z_j)$, and the $\mathbf{r}_j(x_j, y_j, z_j)$ being the position vector of the jth particle with respect to the coordinate system. As (4) and (6) are referenced to the center of the sphere for the evaluation of the terms $\mathbf{E}^r(\mathbf{R}_{0j}, \mathbf{r}_p^j)$, we use the $|\mathbf{R}_{0j}(x_0, y_0, z_0 \mid x_j, y_j, z_j)|$ as r, and we determine the values of θ and φ, termed as θ_{0j} and φ_{0j} for the jth particle, from the known $\widehat{R}_{0j}(x_0, y_0, z_0 \mid x_j, y_j, z_j)$ by some mathematical process.

3. The Synthesized DNG Harvesting System and Results

3.1. The Synthesized Artificial DNG Structure. Applying the theory of Section 2.1, a DNG medium was synthesized with host material, a dielectric with $\varepsilon_h = 1.046$. Regarding Figure 1, the set with the bigger spherical particles, at which the dominant TM_{011} mode is expected to arise, was composed of particles with radius $r_{pe} = 3.75$ mm and $\varepsilon_{rL} = 800$. The set of the smaller spherical particles, which would support the dominant TE_{011} mode, was composed of particles with radius $r_{ph} = 2.56$ mm and $\varepsilon_{rS} = 800$. The value of s is $s = 6.34$ mm. The criterion for selection of the structural parameters values was the DNG performance to appear around 2 GHz, namely, inside the UMTS band and also the size of the spheres and consequently of the cell to not be large. That is why ferroelectric material with $\varepsilon_{rL,S} = 800$ was selected for the dielectric particles. The results of Figures 2 and 3 validate the DNG performance of the synthesized structure. In Figure 2(a), the variation of the effective constants ε_{eff} and μ_{eff} versus frequency, calculated by (1), is depicted, and negative values of both constants are ascertained around 2 GHz. A second verification is provided by the results of Figures 2(b) and 3 which were received via the theory presented in Section 2.2 and depict the variation of field coefficients a_{tn} and b_{tn} versus frequency for both the large and small particles. It is shown that inside the particles of r_{ph} radius, a_{tn} is maximized at 2.035 GHz while the respective b_{tn} coefficient is zero inside all the UMTS frequency band. It means that the electric field intensity, $\mathbf{E}^t$, in the interior to these particles, depends only on $\mathbf{m}_{o1n}^{(1)}$ which has only θ and φ components, and as a result, there is not E_r^t component. Simultaneously, the intensity of the magnetic field, $\mathbf{H}^t$, depends only on $\mathbf{n}_{o1n}^{(1)}$ which has all three spherical components, and so, all three components H_r^t, H_θ^t, and H_φ^t exist.

This performance is clearly shown in Figures 3(c) and 3(d) in which the variation of the field components versus the distance from the particle's center is illustrated, when the amplitude of the incident electric field intensity is $E_0 =$ 1 V/m. So, it is proved that at 2.035 GHz, the particles of radius r_{ph} resonate, supporting the TE_{011} mode. Regarding

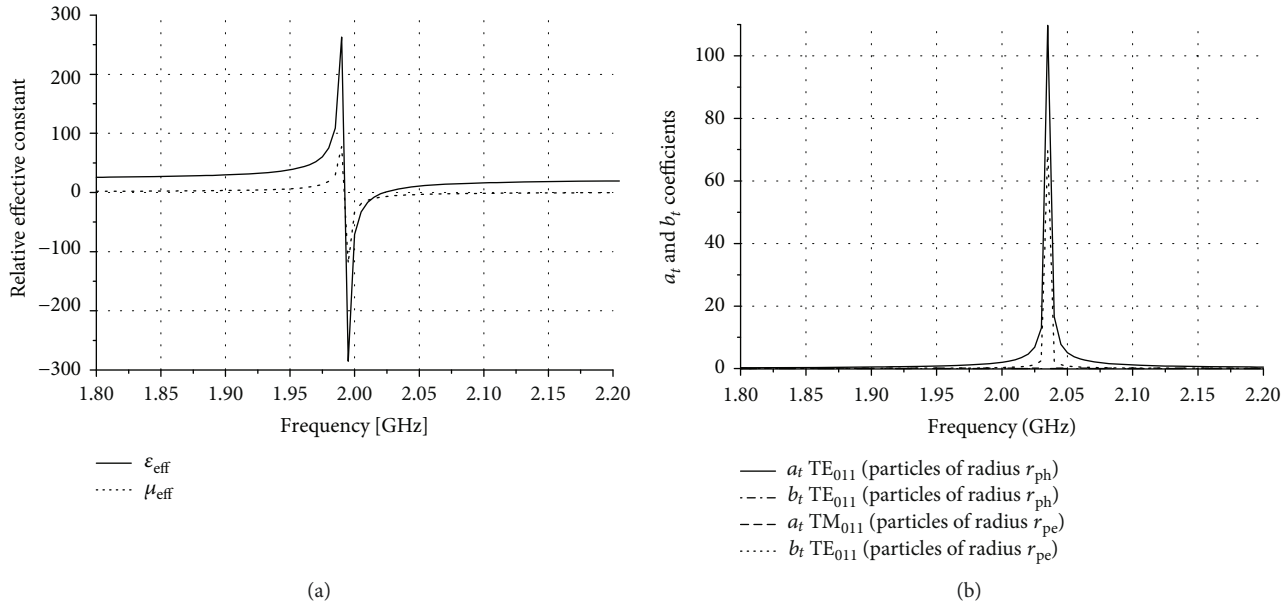

FIGURE 2: Synthesized DNG medium: variation versus frequency of (a) the effective constants ε_{eff} and μ_{eff} and (b) the field coefficients a_{t1} and b_{t1} inside the particles.

the performance of large particles of radius r_{pe}, the coefficient a_{tn} is zeroed inside the UMTS band while the while the b_{tn} is maximized is maximized at 2.035 GHz. It means that $\mathbf{E}^t$ depends only on $\mathbf{n}_{e1n}^{(1)}$ which has all three r, θ, and φ components, and as a result, all the respective three components of the electric field intensity exist. Simultaneously, the intensity of $\mathbf{H}^t$ depends only on $\mathbf{m}_{e1n}^{(1)}$ which has only θ and φ components, and so the H_r^t does not exist. All of them are verified by Figures 3(a) and 3(b), and it is ascertained that at 2.035 GHz, the TM_{011} mode is excited inside the particles of radius r_{pe}.

3.2. Evaluation of Electric Field Intensity inside the DNG Structure. The described performance of the designed DNG structure would be exploited and gain practical value which would make it worthwhile for applications. In the present work, it is introduced as a material that would host sensors for gathering ambient electromagnetic power. The main characteristic that would contribute to the mechanism of energy harvesting is its attribute to create electromagnetic fields of high intensity in its interior. For this purpose, indicative results for the E-field intensity were received theoretically, by (9), and respective ones were received via simulation by a high frequency electromagnetic solver. The results were received for two structures of DNG configuration using, in both, the particles presented in Section 3.1. The first one termed as "Lattice A" is the classical one shown in Figure 1 and the second one termed "Lattice B" is depicted in Figure 4. At the later one, the particles are arranged in a way a little different from that of the classical structure. As shown in Figure 4(b), it is constructed of 3 cells positioned one next to the other at a distance d_{c}.

In both Lattices A and B, the host is extended beyond the lattice of particles for 2 mm along z-direction, namely, the length of the edge D_{hz} is 4 mm larger than the respective edge of the lattice. Considering that the plane wave, propagating along z-axis, impinges on the "front" side of the structure (Figure 4(c)), the distribution of electric field was calculated on the planes tangent to the end of lattice, namely, inside the host and at distances 2 mm away of the "front" and "back" sides. These are the positions at which the wire dipole sensors would be placed. They are assessed as suitable because the field, as shown in Figure 3, has still high intensity values, although smaller than those in the interior of particles. Either way, we cannot exploit the ultra-high field intensity of the particles' interior, because if the dipoles penetrate them, their resonance is prevented.

In accordance to Figure 5, the comparison between the theoretical results and the respective ones of simulation shows a small difference between them coming from the fact that in the theoretical evaluation of the field, by (9), the interaction among the particles was not taken into account, while this parameter is inherently included in the simulation process. For all that, this disagreement is considered not important because the matter was not the convergence of the results. It was known a priori that the theoretical calculations were approximate, but they were made in order that we would have a first assessment for the field intensity level in the host and to verify that it is larger than that of the incident wave, no matter how accurate would be the numerical results. However, as in the following sections are presented, the values of all the parameters included in the estimation of the gathered power and the power available at the output of the rectifier were received via simulation.

Figure 6 illustrates the theoretical results for the field of Lattice A on a plane inside the host and tangentially to the lattice, namely, as in case of Lattice B. Comparing them with those of Figure 5(a), it is ascertained that there is difference concerning the field distribution, and moreover, the field intensity in case of Lattice A is smaller than that of Lattice

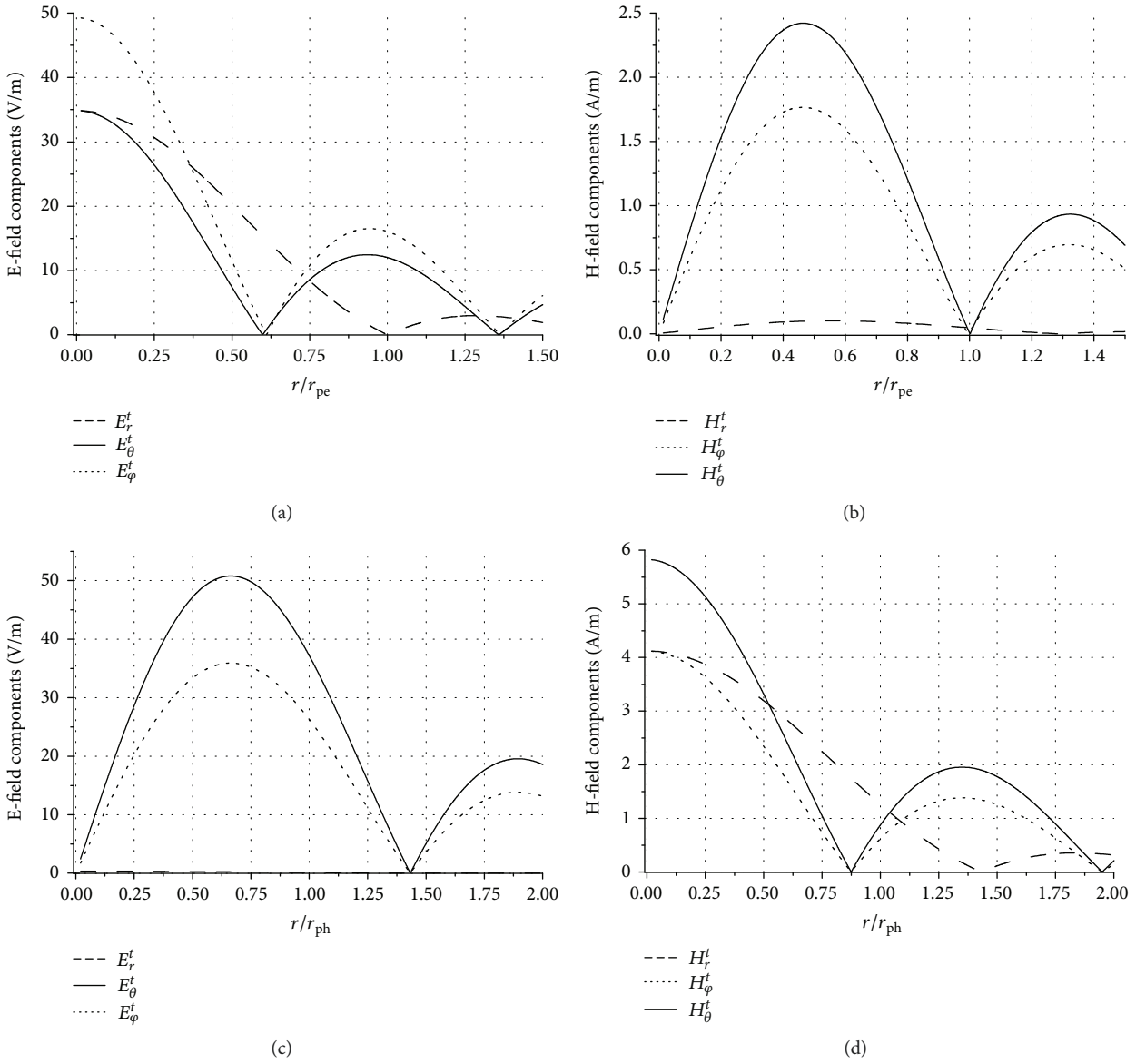

FIGURE 3: Field components distribution inside the particles for $E_0 = 1$ V/m. (a) and (b) TM_{011} mode inside particles of radius r_{pe}. (c) and (d) TE_{011} mode inside particles of radius r_{ph}. The diagrams were plotted for polar angles $\theta = \pi/4$ and $\varphi = \pi/4$.

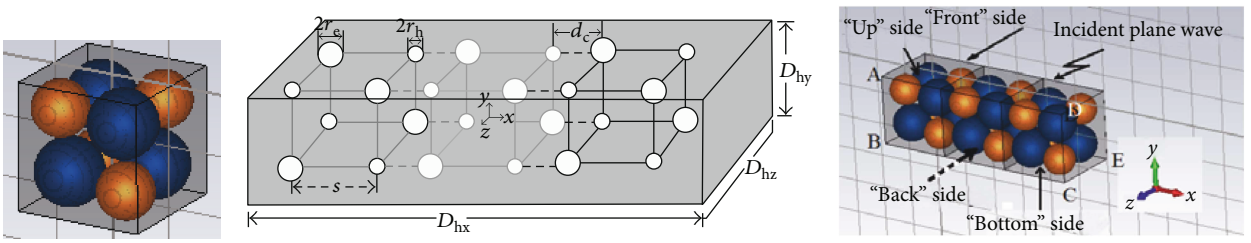

FIGURE 4: The medium designed to behave as DNG material around 2 GHz. (a) The unit cell of 8 particles. (b) The configuration of "Lattice B" composed of 3 adjacent cells, $s = 6.34$ mm, $r_e = 3.75$ mm, $r_h = 2.56$ mm, $d_c = 1$ mm, total lattice size = 43.34 mm × 13.78 mm × 13.78 mm, and size of lattice plus host: $D_{hx} = 44.34$ mm, $D_{hy} = 14.78$ mm, and $D_{hz} = 17.78$ mm. (c) the 3D pattern of the Lattice B.

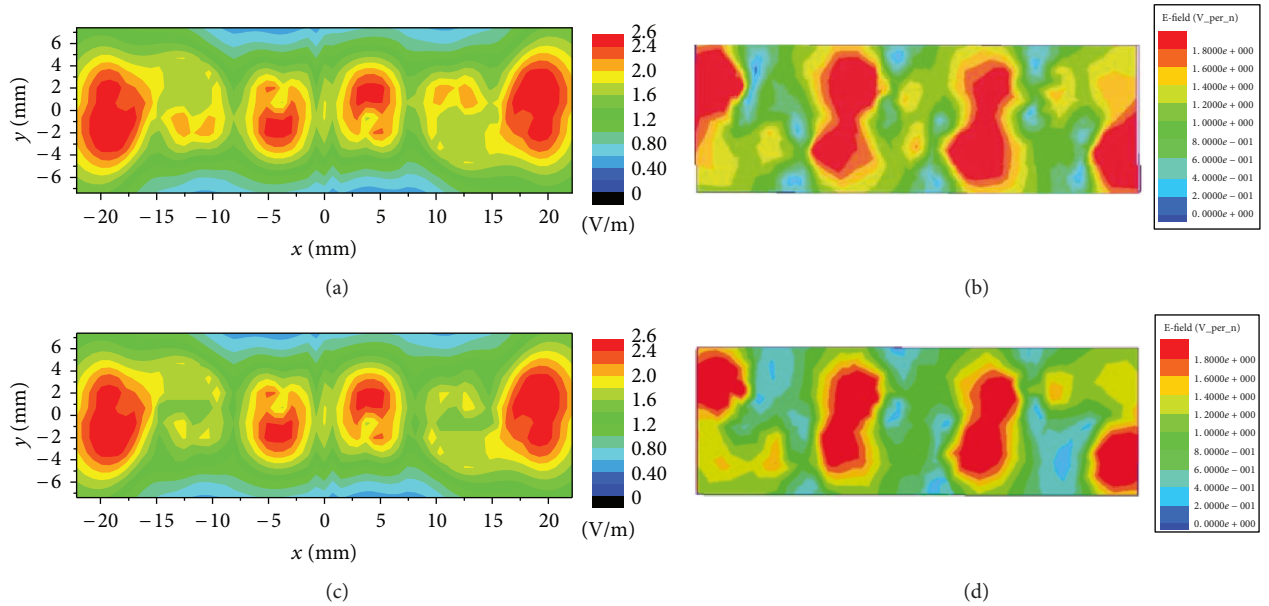

Figure 5: Lattice B: results received (a) and (c) theoretically and (b) and (d) via simulation. The absolute value of the electric field intensity on planes inside the host and 2 mm off from (a) and (b) the "front side" on which the x-polarized plane wave impinges perpendicularly and (c) and (d) the "back side" of the slab. Amplitude of the plane wave $E_0 = 1$ V/m and $f = 2.035$ GHz.

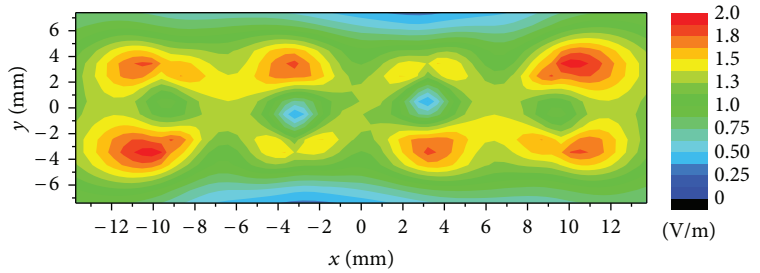

Figure 6: Lattice A: results received theoretically. The absolute value of the electric field intensity on planes inside the host and 2 mm off from "front side" on which the x-polarized plane wave of $E_0 = 1$ V/m and $f = 2.035$ GHz impinges perpendicularly. Geometry of Lattice A: $s = 6.34$ mm, $r_e = 3.75$ mm, and $r_h = 2.56$ mm and size of lattice plus host: $D_{hx} = 27.46$ mm, $D_{hy} = 14.78$ mm, and $D_{hz} = 17.78$ mm.

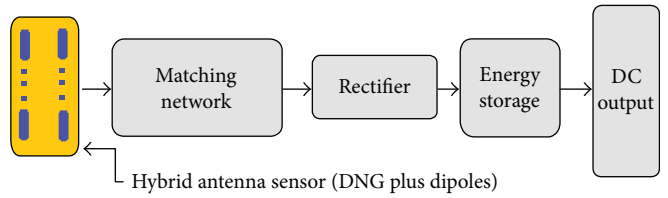

Figure 7: The scheme of an ordinary harvesting system with the hybrid antenna sensor (DNG plus dipoles).

B. So, the study about the harvesting of electromagnetic power with dipole sensors was made using Lattice B.

3.3. The Proposed Harvesting Scheme and the Power Harvesting

3.3.1. The Proposed Harvesting Scheme. As mentioned in Section 1, the main grades of a global harvesting system are, besides the antenna sensor, a matching network, the rectifier, and the energy storage (Figure 7). In the present work, antenna sensor is proposed as the synthesized hybrid sensor of the designed DNG with Lattice B and the incorporated dipoles. Numerical results for the effectiveness of the global hybrid sensor are presented in the following subsection.

3.3.2. Linear Dipole Sensors inside the DNG Structure and Power Harvesting. The study and the results of this subsection regard an assessment of the increase of the gathered power by linear dipoles when positioned inside the host, in front or/and back of the Lattice B, instead of being positioned

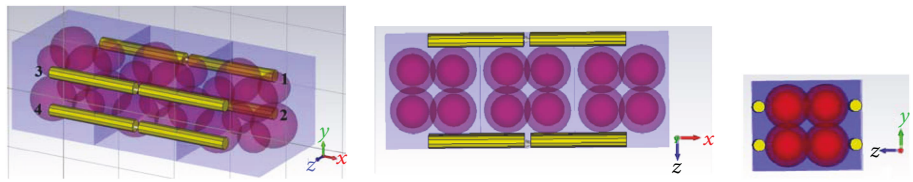

(a) (b) (c)

Figure 8: Dipole' s length 30 mm and radius 1 mm. The dipoles' positions along y-direction, measured from the "bottom" side, are 10.56 mm for dipoles 1 and 3 and 4.22 mm for dipoles 2 and 4. Total scheme size: 44.34 mm × 14.78 mm × 17.78 mm. (a) 3D view, (b) top view, and (c) side view.

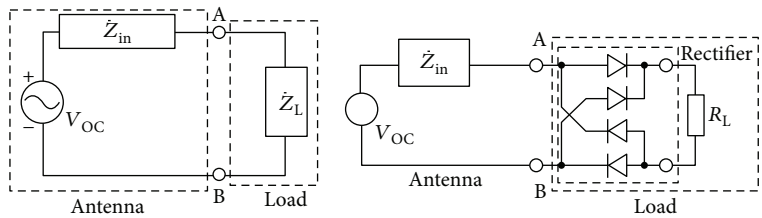

(a) (b)

Figure 9: (a) General equivalent circuit of an antenna and a load connected at its input. (b) The equivalent circuit of each dipole, with or without DNG, connected to a full wave rectifier with resistive load R_L at its output ports.

in free space. An indicative proposed scheme is shown in Figure 8, where 4 dipoles are employed, while more or less of them could be used. Dipoles 1 and 2 are positioned inside the host, 2 mm from the "front side" of the Lattice B (Figure 4(c)) and tangentially to the spheres, while dipoles 3 and 4 are positioned inside the host 2 mm from the "back side" and are also tangentially to the respective spheres.

The entire process of effective energy harvest has two basic steps. One of them is the dipole sensor to gather power as much as possible and the second one is to transfer as much as possible amount of the gathered power to the rectifier and the storage unit. Concerning the first step, the synthesized DNG slab is used for the enhancement of the scavenging, and for the power estimation, the antenna theory is applied [23]. It is well known that when an antenna works as a receiver, it plays the role of a voltage source for the load at which it transfers the received power. In the respective equivalent electric circuit shown in Figure 9, V_{oc} is the antenna voltage induced at the open-circuited antenna input terminals, Z_{in} is the complex input impedance of the antenna, and Z_L is the impedance of any load connected to the antenna's input. The power transferred from the antenna to the load depends on all three above parameters and can be calculated by them.

So, in the present problem, the first step is to calculate the V_{oc} at the input of each dipole. Two schemes were investigated. The first one includes the DNG slab and only one dipole, namely, the dipole 1 or the dipole 3, in accordance with Figure 8.

The results of Figure 10(a) were received via simulation and show the variation of the dipoles' V_{oc} versus frequency. The wave was propagating along $+z$-axis, and its direction of arrival (DoA), considered with respect to this axis, was 0 deg namely, it impinges perpendicularly to the "front" side of the DNG (Figure 4(c)). For comparison, the V_{oc} for the same dipoles positioned in free space is presented. In all cases, the magnitude of the incident electric field intensity was considered, $E_0 = 1$ V/m. It is ascertained that the V_{oc} in case of one dipole in free space is almost constant, having value about −37 dBVolt (14.12 mV), while in case of dipole DNG, it strongly fluctuates, appearing values much larger or much lower than this value at various frequency ranges inside UMTS band. So, for an estimation to be made, the average V_{oc}, termed V_{ocave}, over 10^3 frequency values in the entire band was calculated and was found −33.64 dBVolt (20.79 mV), in case of sole dipole 1 plus DNG while in case of sole dipole 3 plus DNG it was found equal to −34.35 dBVolt (19.16 mV). The small difference between the results of two positions comes from the small difference of field distribution in front and back sides of the slab. What is interesting is that for both dipoles' positions, the V_{ocave} is larger than in the case of dipole in free space. The results are presented in detail in Table 1.

In Figure 10(b), respective results for V_{oc} versus frequency of the arrangement of 4 dipoles positioned as shown in Figure 8 are presented. For comparison, results for these four dipoles in free space, namely, without the DNG, are depicted. Results for dipoles 1 and 3 are only presented, for both cases, because dipoles 2 and 4 exhibit V_{oc} values equal to those of dipoles 1 and 3, respectively, due to their respective positions which are symmetrical regarding the DNG slab. It is pointed out that the V_{oc} values of dipoles 1 or 3 are not equal to those in case at which anyone of them was alone, as in Figure 10(a) is shown, due to mutual coupling among them when all four are present. In detail, it is due to the fact that the V_{oc} of each one comes not only from the impinging plane wave and the field of DNG but also from the reradiation of the rest 3 dipoles. In this case, the V_{ocave}

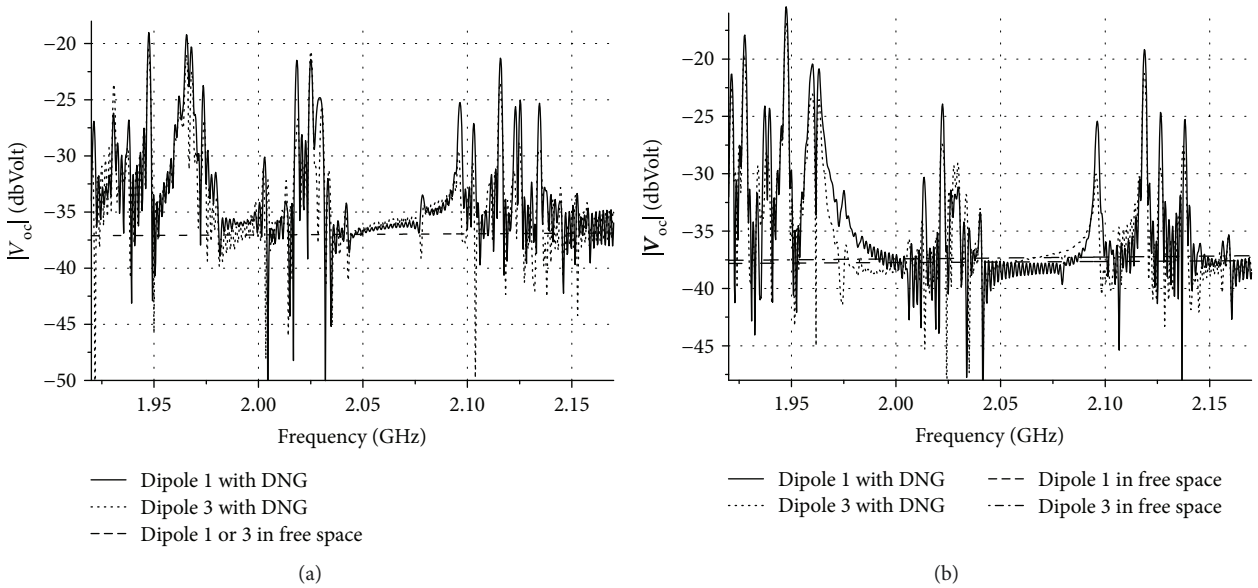

Figure 10: Absolute values of the voltage induced at the open input terminal of dipoles with DNG and free space (a) only one dipole (1 or 3) and (b) all 4 dipoles present, results for 1 and 3. DoA: 0 deg.

Table 1: V_{ocave} values at the open-circuited input terminals of the dipoles. Average values over the UMTS band. DoA: 0 deg.

	With DNG	In free space
	1 dipole	
Dipole 1	−33.64 dBVolt	−37 dBVolt
Dipole 3	−34.35 dBVolt	−37 dBVolt
	4 dipoles	
Dipole 1	−34.98 dBVolt	−37.69 dBVolt
Dipole 3	−35.49 dBVolt	−37.35 dBVolt

values are −34.98 dBVolt (17.82 mV) for dipole 1 and −35.49 dBVolt (16.8 mV) for dipole 3 in presence of DNG. The respective values in free space are −37.69 dBVolt (13.04 mV) for dipole 1 and −37.35 dBVolt (13.57 mV) for dipole 3 (Table 1).

The next step in the assessment of the capability of the system dipoles-DNG to work effectively as a harvester of ambient electromagnetic power is to estimate the amount of the gathered power which would be transferred to a load Z_{L}. This load, in practice, would be the rectifier with its output connected to a load R_{L} or to the energy storage unit. In accordance to the equivalent circuit of Figure 9(a), the complex current of the loop is $\dot{I}(f) = \dot{V}_{\text{oc}}(f)/(\dot{Z}_{\text{in}}(f) + \dot{Z}_{\text{L}})$, and the active power in watts available to $\text{Re}(\dot{Z}_{\text{L}})$ is $P_{\text{L}} = \text{Re}(\dot{Z}_{\text{L}})(|\dot{V}_{\text{oc}}(f)|/(|\dot{Z}_{\text{in}}(f) + \dot{Z}_{\text{L}}|))^2$.

In the present application, the power gathered by the hybrid antenna, in order to be stored, is firstly rectified. So, estimation was made for a basic full wave rectifier as depicted in Figure 9(b). For the rectifier, the Schottky diode HSMS-285C [24] was considered. Its equivalent circuit is a resistor of 2.5 ohms in series with a capacitance of $C_{\text{D}} = 0.88$ pF. So, the complex impedance of the diode is $\dot{Z}_{\text{D}}(f) = 2.5 + 1/(j2\pi f C_{\text{D}})$. The total $\dot{Z}_{\text{L}}$ of the rectifier plus the resistor R_{L} connected at its output terminals, during each half period time of the signal, is $\dot{Z}_{\text{L}}(f) = 2\dot{Z}_{\text{D}}(f) + R_{\text{L}}$. The power $P_{\text{L}}(f)$ available at resistor R_{L} is

$$P_{\text{L}}(f) = R_{\text{L}} \left(\frac{|\dot{V}_{\text{oc}}(f)|}{|\dot{Z}_{\text{in}}(f) + \dot{Z}_{\text{L}}(f)|} \right)^2 \quad (10)$$

Generally, with intend this power to be maximized, a matching network would be applied between the antenna's terminals and the input of the rectifier, at points A and B (Figure 9(b)). However, at the proposed antenna scheme, the results of simulation show that the real part of $\dot{Z}_{\text{in}}(f)$, of each dipole, appears abrupt variations inside the UMTS band. The same is valid for the imaginary part, but this part is almost zero inside large frequency subareas, and this behavior, showing resonance, is judged satisfactorily. The aforementioned performance is depicted in Figure 11, which illustrates the real and imaginary part of the input impedance of all four dipoles positioned in front and back DNG side (Figure 8) and the respective ones in free space. In case of more than one dipole, the input impedance of ith dipole is $Z^i_{\text{in}} = \sum_{j=1}^{4} Z_{ij}$, where Z_{ij} is the mutual impedance between ith and jth dipoles calculated via simulation. Due to the symmetrical positions of them, relatively to DNG and also in free space, the mutual impedances Z_{ij} and Z_{ji} are of equal value and consequently the same holds for Z^i_{in}, $i = 1,2,3,4$. It is pointed out that the input impedance, of each one of the dipoles, without the presence of the rest 3 ones, varies versus frequency with the same way having however different values.

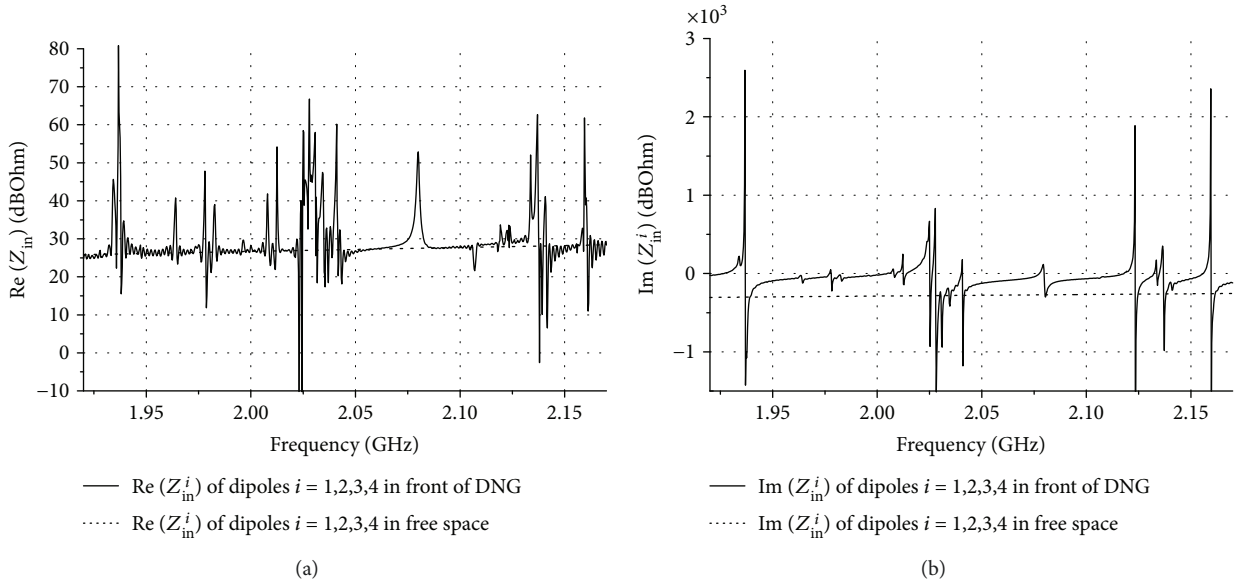

FIGURE 11: Input impedance of dipoles 1 to 4 with and without DNG slab. (a) Real part. (b) Imaginary part.

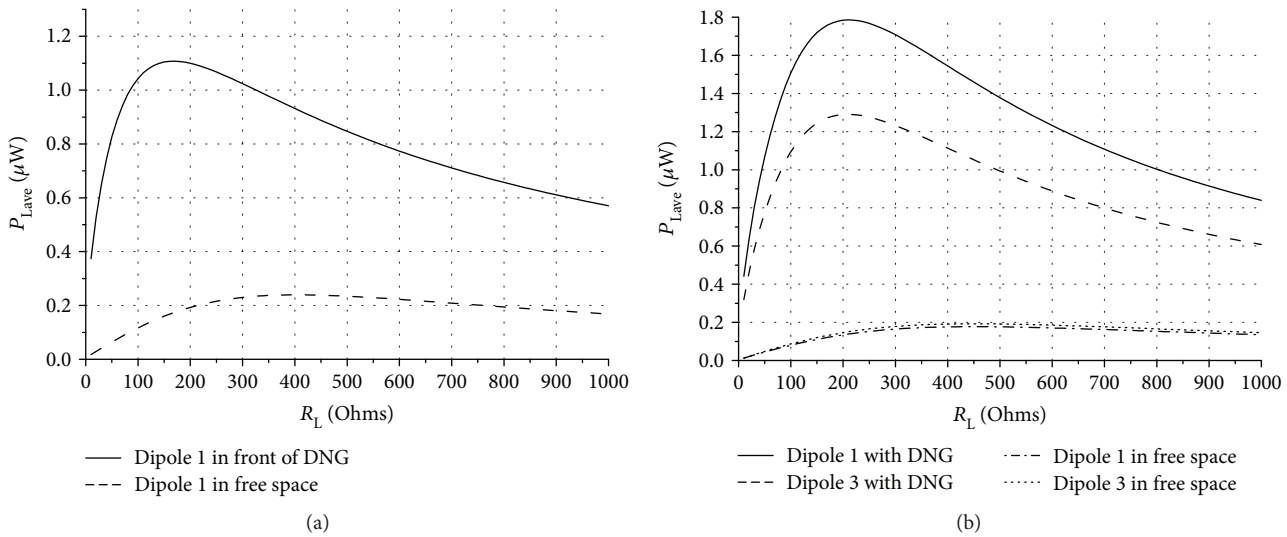

FIGURE 12: Average power per dipole at R_L over the UMTS band versus R_L for dipoles with and without DNG slab. (a) Only one dipole. (b) Four dipoles.

As previously discussed, a matching network was not used. The estimation of the power gathered from the antenna system and being available to the resistor R_L, in case of one or four dipoles with the DNG slab or in free space, was made considering that each dipole is connected to its own rectifier and using (10). An alternative solution would be the combination of the signals of two dipoles, for example, the signal of dipole 1 with that of dipole 2 and the signals of dipoles 3 and 4 and then the leading of them to a rectifier. In this way, one rectifier per two dipoles would be used. In any case, investigation for the proper value of R_L in order for $P_L(f)$ to be maximized is necessary. Due to the dependence of P_L on the frequency, it was calculated at 10^3 frequency values in the UMTS band, and the average value P_{Lave} was estimated. The same was repeated for a large number of different R_L values. The results are presented in Figure 12, which includes results for only dipole 1 with and without DNG slab and results for dipoles 1 and 3 with and without the slab for the arrangement of 4 dipoles. In the last case, the presented results regard substantially all four dipoles, because those of dipole 1 are similar to those of dipole 2 and those of dipole 3 are equal to those of dipole 4.

From Figure 12(a), it is concluded that in case of one dipole, the R_L value which maximizes the P_{Lave} is 160 ohms when DNG is present and 350 ohms in free space. The results of Figure 12(b) were received from the arrangement of all four dipoles and show that the R_L value which maximizes the P_{Lave} is 200 ohms for the dipoles 1 and 3 in presence of DNG and 400 ohms in free space. Differences also appear with respect to the maximum P_{Lave} values. The numerical

Table 2: Average power available per dipole on the load R_L at the output of the rectifier.

	Only dipole 1		
	P_{Lave}^{DNG}, R_L = 160 ohms	$P_{Lave}^{fr\ space}$, R_L = 350 ohms	$P_{Lave}^{DNG}/P_{Lave}^{fr\ space}$ (dB)
	1.1 μW	0.23 μW	6.79
	4 dipoles		
	P_{Lave}^{DNG}, R_L = 200 ohms	$P_{Lave}^{fr\ space}$, R_L = 400 ohms	
Dipole 1	1.78 μW	0.176 μW	10.05
Dipole 3	1.29 μW	0.191 μW	8.29

results are presented in detail in Table 2 and prove that either one dipole or all four dipoles are used, when they are incorporated in the DNG; the power available to R_L, per dipole, is greater by several dBs than that obtained by the same dipoles arranged in free space.

In order to complete the assessment for the performance of the introduced hybrid sensor, linear dipole DNG and its effectiveness not only to gather ambient RF power but to transfer it to the rectifier and also to obtain to excite the rectifying unit; the rectifier's input voltage, termed V_{inrect}, was calculated. It is determined as $\dot{V}_{inrect}(f) = \dot{V}_{oc}(f)\dot{Z}_L/(\dot{Z}_{in}(f) + \dot{Z}_L)$ in accordance to the equivalent circuit shown in Figure 9(a). Moreover, given that in practice the DoA of the incoming waves, measured in degrees, could potentially have any other value besides that of 0 deg, results versus various DoA values were received by simulation. In all cases, the electric field intensity of the incident wave was 1 Volt/m. The results, presented in the following, concern, indicatively, the case of "Dipole 1," in front of the DNG and in free space, while the performance of the rest of dipoles is similar. At first, in Figure 13, the average voltage value, V_{ocave}, versus the DoA of the incident wave at the open input terminals of the dipole 1 with and without DNG is presented. It is observed that V_{ocave} values of the scheme dipole DNG remains higher enough than that of the dipole in free space for all the DoAs of the incident waves. Especially in the case of 90 deg incidence, at which the V_{oc} of the dipole in free space is, as expected, almost zero, when the dipole is in front of the DNG, a V_{ocave} about 7 mVolts is obtained. It comes from the field developed around the DNG particles in the vicinity of which the dipole is placed.

Figures 14(a) and 14(b) depict the variation of V_{inrect} versus frequency for two DoAs, for the sensor dipole 1-DNG. As expected, it fluctuates inside the UMTS band. The information for the minimum and maximum V_{inrect} values of this fluctuation is presented in Table 3. Additional results concerning the average, over the UMTS band, voltage value at the input terminals of the rectifier, versus DoA, are presented in Figure 14(c). They show that the dipole DNG is capable of ensuring voltage values higher than those in the case of dipole in free space, for any DoA.

Table 3 includes also additional information for the proportion of the magnitude of the average total power S_{tot}^{ave}, available to the rectifier (S_{rect}^{ave}). Both quantities were calculated in accordance to the equivalent circuit of Figure 9(a) at which the load $\dot{Z}_L$ stands for the rectifier. The results were

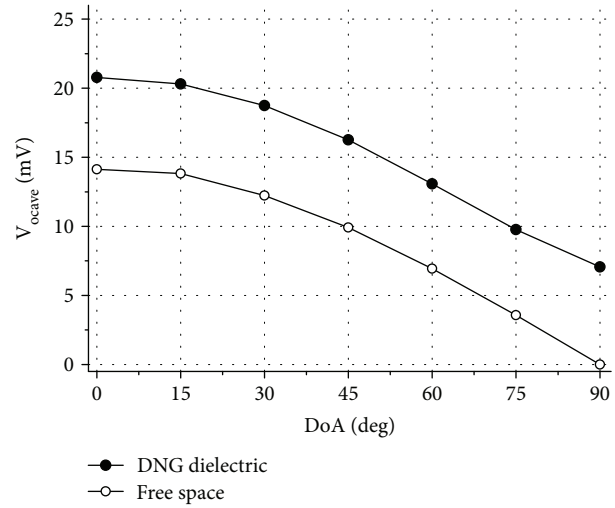

Figure 13: "Dipole 1" in front of the DNG and in free space: V_{ocave} (mVolts) values, calculated over the UMTS band, at the open-circuited input terminals of the dipole, versus the direction of arrival (DoA) of the incoming wave. DoA is considered with respect z-axis.

received for the hybrid sensor and for the dipole in free space. The values are averaged over the UMTS band and the rectifier's output was connected to the respective R_L by which maximum P_L is obtained. The results show that the hybrid sensor holds high capability of transferring the captured ambient RF power to the rectifier for any DoA of the incident wave. It is pointed out that this capability seems to be greater in case of the dipole in free space and for DoAs larger than 45 deg. However, in absolute values, the transferred power is much smaller because in free space the dipoles gather significantly smaller amount of power, as shown in Table 2 and in Figures 12–14.

4. Conclusions

The work focuses on the feasibility of enhancing the performance of an ordinary antenna scheme, as wire dipoles, by employing DNG metamaterial structures in order to make it more efficient for harvesting of ambient electromagnetic RF energy. A DNG structure was designed for the UMTS band, and linear wire dipoles were incorporated with it, thus constituting a hybrid compact ambient RF power harvester of total size 44.34 mm × 14.78 mm × 17.78 mm. The proceeded theoretical analysis of the DNG proved that when it

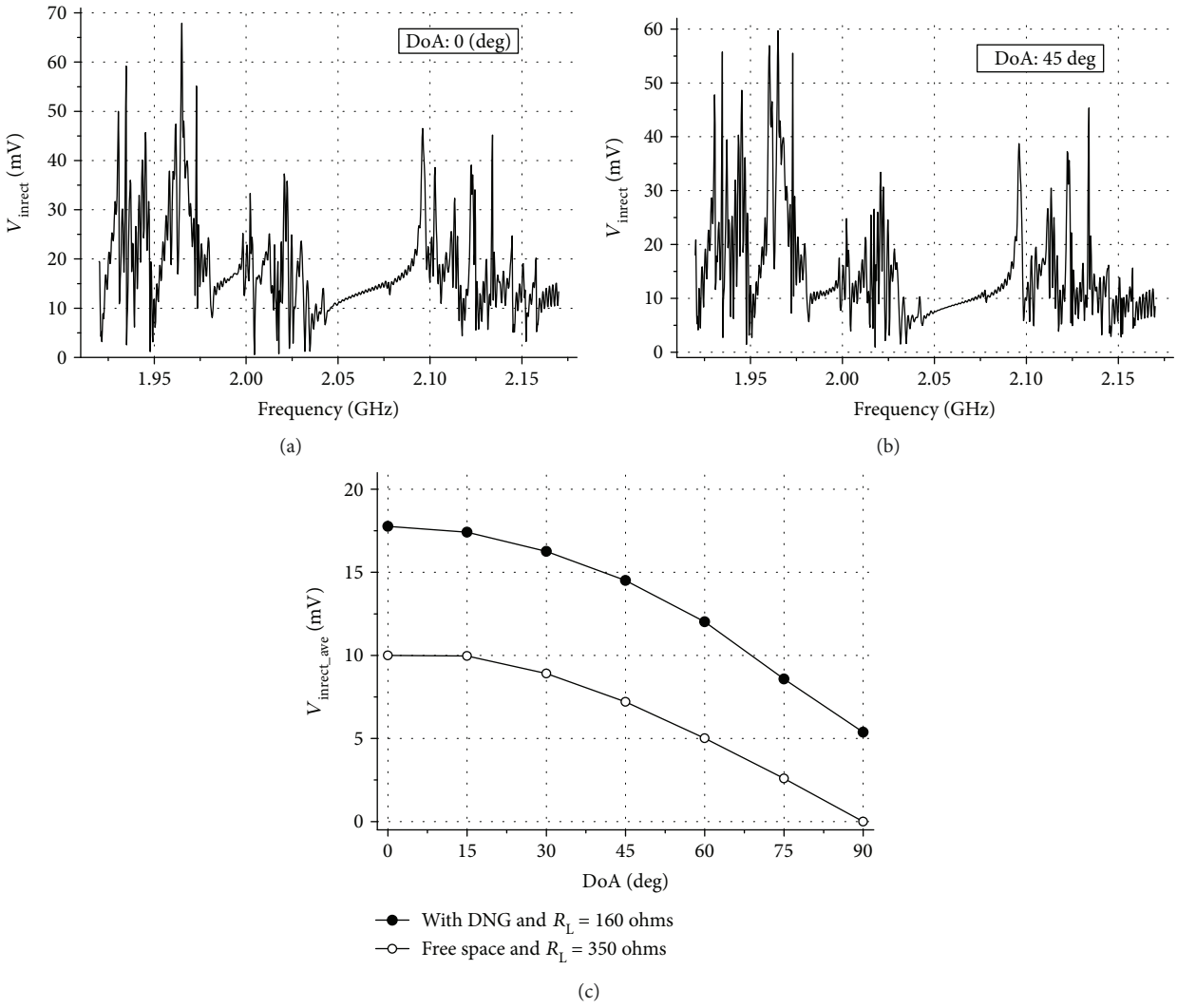

Figure 14: (a) and (b) Results versus frequency, for the input voltage of the rectifier of the sensor "Dipole 1-DNG" when connected to the full wave rectifier in cases of DoA 0 deg and 45 deg. Rectifier's output is connected to the R_L by which maximum P_L is obtained (c) available average voltage values, calculated over the UMTS band, at the input of the rectifier, for the sensor "Dipole 1-DNG" and for the same dipole in free space. Electric field intensity of the incident wave 1 V/m.

Table 3: Results versus DoA, of the "Dipole 1," positioned in front of the DNG and in free space, when connected to the full wave rectifier. Proportion of the magnitude of the average total power S_{tot}^{ave}, available to the rectifier (S_{rect}^{ave}). The values are averaged over the UMTS band, and the rectifier's output is connected to the R_L by which maximum P_L is obtained.

DoA (deg)	DNG, R_L = 160 ohms		$S_{rect}^{ave}/S_{tot}^{ave}$ (%)	
	V_{inrect_max}	V_{inrect_min}	DNG, R_L = 160 ohms	Free space, R_L = 350 ohms
0	67.9	0.59	77.7	72.6
15	66.9	0.83	76.8	72.5
30	64	0.90	75.1	72.5
45	59.71	0.94	72.3	72.5
60	57.89	0.44	70.0	72.5
75	57.46	0.51	67.9	72.4
90	56	0.11	67.8	72.4

is illuminated by a plane electromagnetic wave, areas of high intensity field are created in its interior. These areas are suitable positions for placing the dipole antenna sensors in order for the gathered power to be enhanced. Analytical results were received and show the capability of dipoles to exhibit at their open-circuited input terminals, induced voltages more than 3 dBs larger than they could obtain in free space, and it is valid for all directions of arrival of the incident wave. It is worth to mention that when the wave impinges almost with DoA 90 deg, namely, propagates along the dipoles' axis, the input voltage is practically zero when the dipoles are in free space while in the vicinity of the DNG voltage of several mVolts is obtained. Moreover, the results concerning the gathered power, that is available at the output of the rectifier, are, per dipole, about 6.8 dB to 10 dB greater than it would be without the presence of the DNG. The results also show that the available voltage at the input of the rectifier, at the sensors

dipole-DNG, is satisfactory higher than it is at dipoles in free space, and this superiority is observed at all DoAs.

It is pointed out, generally, that due to the sensor's configuration, namely, the capability of positioning dipole sensors simultaneously in front and back of the Lattice B, is an advantage, as duplicates the number of sensors and additionally, the power each one of them gathers could be added up with that of the others giving a total power much greater than that of only one dipole.

Finally, a general conclusion could be that the composed hybrid sensor of the triad of DNG cells and their dipoles could be used as primary unit for structuring large panels utilizing a large number of them and which would strongly increase the amount of the gathered ambient RF power.

Conflicts of Interest

The authors declare that they have no conflicts of interest.

References

[1] S. Keyrouz, H. J. Visser, and A. G. Tijhuis, "Ambient RF energy harvesting from DTV stations," in *2012 Loughborough Antennas & Propagation Conference (LAPC)*, pp. 1–4, Loughborough, UK, November 2012.

[2] H. J. Visser, A. C. F. Reniers, and J. A. C. Theeuwes, "Ambient RF energy scavenging: GSM and WLAN power density measurements," in *2008 38th European Microwave Conference*, pp. 721–724, Amsterdam, Netherlands, October 2008.

[3] S. Kim, R. Vyas, J. Bito et al., "Ambient RF energy-harvesting technologies for self-sustainable standalone wireless sensor platforms," *Proceedings of the IEEE*, vol. 102, no. 11, pp. 1649–1666, 2014.

[4] S. Sudevalayam and P. Kulkarni, "Energy harvesting sensor nodes: survey and implications," *IEEE Communications Surveys & Tutorials*, vol. 13, no. 3, pp. 443–461, 2011.

[5] J. Zhang, Y. Huang, and P. Cao, "A wideband cross-dipole rectenna for rf wireless harvesting," in *2013 7th European Conference on Antennas and Propagation (EuCAP)*, pp. 3063–3067, Gothenburg, Sweden, April 2013.

[6] B. L. Pham and A.-V. Pham, "Triple bands and high efficiency rectifier design for RF energy harvesting at 900, 1900 and 2400 MHz," in *2013 IEEE MTT-S International Microwave Symposium Digest (MTT)*, pp. 1–3, Seattle, WA, USA, 2013.

[7] A. Collado and A. Georgiadis, "Conformal hybrid solar and electromagnetic (EM) energy harvesting rectenna," *IEEE Transactions on Circuits and Systems I: Regular Papers*, vol. 60, no. 8, pp. 2225–2234, 2013.

[8] F. Zhang, X. Liu, F.-Y. Meng et al., "Design of a compact planar rectenna for wireless power transfer in the ISM band," *International Journal of Antennas and Propagation*, vol. 2014, Article ID 298127, 9 pages, 2014.

[9] S. Shrestha, S. R. Lee, and D.-Y. Choi, "A new fractal-based miniaturized dual band patch antenna for RF energy harvesting," *International Journal of Antennas and Propagation*, vol. 2014, Article ID 805052, 9 pages, 2014.

[10] A. Nimo, D. Grgic, and L. M. Reindl, "Ambient electromagnetic wireless energy harvesting using multiband planar antenna," in *International Multi-Conference on Systems, Sygnals & Devices*, pp. 1–6, Chemnitz, Germany, March 2012.

[11] S. Ladan, N. Ghassemi, A. Ghiotto, and K. Wu, "Highly efficient compact rectenna for wireless energy harvesting application," *IEEE Microwave Magazine*, vol. 14, no. 1, pp. 117–122, 2013.

[12] H. Sun, Y.-X. Guo, M. He, and Z. Zhong, "A dual-band rectenna using broad-band yagi antenna array for ambient RF power harvesting," *IEEE Antennas and Wireless Propagation Letters*, vol. 12, pp. 918–921, 2013.

[13] T. Almoneef and O. M. Ramahi, "A 3-dimensional stacked metamaterial arrays for electromagnetic energy harvesting," *Progress In Electromagnetics Research*, vol. 146, pp. 109–115, 2014.

[14] N. Zhu, P. Jin, R. W. Ziolkowski, and H. Xin, "Design of a GPS L1 rectenna by using a metamaterial-inspired eclectically small antenna," in *2011 IEEE International Symposium on Antennas and Propagation (APSURSI)*, pp. 1081–1084, Spokane, WA, USA, July 2011.

[15] M. Zeng, A. S. Andrenko, X. Liu, Z. Li, and H.-Z. Tan, "A compact fractal loop rectenna for RF energy harvesting," *IEEE Antennas and Wireless Propagation Letters*, vol. 16, pp. 2424–2427, 2017.

[16] A. Z. Ashoor and O. M. Ramahi, "Dielectric resonator antenna arrays for microwave energy harvesting and far-field wireless power transfer," *Progress In Electromagnetics Research C*, vol. 59, pp. 89–99, 2015.

[17] A. Karampatea and K. Siakavara, "Employment of DNG dielectric structures in ambient microwave energy harvesting systems," in *2016 5th International Conference on Modern Circuits and Systems Technologies (MOCAST)*, pp. 1–4, Thessaloniki, Greece, May 2016.

[18] X. Zhang, H. Liu, and L. Li, "Tri-band miniaturized wide-angle and polarization-insensitive metasurface for ambient energy harvesting," *Applied Physics Letters*, vol. 111, no. 7, article 071902, 2017.

[19] C. L. Holloway, E. F. Kuester, J. Baker-Jarvis, and P. Kabos, "A double negative (DNG) composite medium composed of magnetodielectric spherical particles embedded in a matrix," *IEEE Transactions on Antennas and Propagation*, vol. 51, no. 10, pp. 2596–2603, 2003.

[20] A. Ahmadi and H. Mosallei, "All-dielectric metamaterials: double negative behavior and bandwidth-loss improvement," in *2007 IEEE Antennas and Propagation International Symposium*, pp. 5527–5530, Honolulu, HI, USA, June 2007.

[21] I. Vendik, O. Vendik, and M. Odit, "Isotropic artificial media with simultaneously negative permittivity and permeability," *Microwave and Optical Technology Letters*, vol. 48, no. 12, pp. 2553–2556, 2006.

[22] J. A. Stratton, *Electromagnetic Theory*, McGraw-Hill, New York, NY, USA, 1941.

[23] C. A. Balanis, *Antenna Theory: Analysis and Design*, John Wiley & Sons, Hoboken, NJ, USA, 4th edition, 2016.

[24] Avago TechnologiesData sheet HSMS-285x.